Journal of Alloys and Compounds xxx (2014) xxx–xxx

Contents lists available at ScienceDirect

Journal of Alloys and Compounds

journal homepage: www.elsevier.com/locate/jalcom

Enhancement of negative capacitance effect in $(CoFeZr)_x(CaF_2)_{(100-x)}$ nanocomposite films deposited by ion beam sputtering in argon and oxygen atmosphere

T.N. Koltunowicz [a,*], P. Zhukowski [a,*], V. Bondariev [a], A. Saad [b], J.A. Fedotova [c], A.K. Fedotov [d], M. Milosavljević [e], J.V. Kasiuk [c]

[a] Lublin University of Technology, 20-618 Lublin, Poland
[b] Al Balqa Applied University, Physics Department, P.O. Box 4545, Amman 11953, Jordan
[c] National Center for Particles and High Energy Physics of Belarusian State University, 220040 Minsk, Belarus
[d] Belarusian State University, 220030 Minsk, Belarus
[e] VINČA Institute of Nuclear Sciences, Belgrade University, P.O. Box 522, 11001 Belgrade, Serbia

ARTICLE INFO

Article history:
Available online xxxx

Keywords:
Electronic transport
Hopping conductance
Nanocomposites
Percolation

ABSTRACT

The paper presents frequency f and temperature T_p dependences of phase shift angle Θ, admittance σ and capacitance C_p for the as-deposited and annealed $(CoFeZr)_x(CaF_2)_{(100-x)}$ nanocomposite films deposited by ion-beam sputtering of a compound target in a mixed argon–oxygen gas atmosphere in vacuum chamber. The studied films presented metallic FeCoZr "cores" covered with FeCo-based oxide "shells" embedded into oxygen-free dielectric matrix (fluorite). It was found for the metallic phase content within the range of 52.2 at.% $\leqslant x \leqslant$ 84.3 at.% in low-f region that Θ values were negative, while in the high-f region we observed the $\Theta < 0^o$. It was obtained that the f-dependences of capacitance module displayed minimum at the corresponding frequency when the $\Theta(f)$ crossed its zero line $\Theta = 0^o$. It was also observed that the $\sigma(T_p)$ dependence displayed the occurrence of two minima that were related to the values of $\Theta_1 = 90°$ (the first minimum) and of $\Theta_2 = -90°$ (the second one). Some possible reasons of such behavior of $(CoFeZr)_x(CaF_2)_{(100-x)}$ nanocomposite films are discussed.

1. Introduction

It is well established that metal–dielectric nanocomposites often reveal very specific mechanical [1,2], magnetic [3–5], and also electrical [6–8] properties, particularly effect of "negative capacitance" [9–15]. This effect is related to inductive-like contribution to the admittance frequency dependences (f) and for the first time was observed in semiconductor heterogeneous structures [9–12]. Our previous investigations of granular nanocomposite films, where metallic (CoFeZr) nanoparticles were embedded into *amorphous oxygen-containing* dielectric matrixes (Al_2O_3 or PZT), also revealed "negative capacitance" effect [13,14]. Particularly, observed positive values of phase-shift angles Θ detected during (f) measurements using RCL-meter were interpreted as phase current oscillations due to AC voltage applied that are characteristic of the RLC circuits.[1] In an ideal case of the RLC circuit with the zero-resistance inductive element, voltage should lead current by the angle of $\Theta = 90°$.

As was shown in [13,14], in these nanocomposite films Θ values were observed in the range $-90° \leqslant \Theta < 0°$ within the low-f range and $0° < \Theta \leqslant 90°$ at the high-f values. This means that in the studied nanocomposites the reactive part of admittance presents a complex superposition of the capacitive and inductive contributions. This is also agreed with the behavior of $C_p(f)$ dependences every of which reached the local minimum at some frequency f_0 appropriated to $\Theta = 0°$. This means the occurrence of voltage resonance at the frequency

$$f_0 = \frac{1}{2\pi\sqrt{LC}} \tag{1}$$

and compensation of opposite-phase voltages of the capacitive and inductive contributions, that resulted in, as observed in [13,15], the reaching of minimum on $C_p(f)$ dependences.

As a rule, the highest inductive-like contributions to admittance were observed in $(CoFeZr)_x(Al_2O_3)_{(100-x)}$ and $(CoFeZr)_x(PZT)_{(100-x)}$ nanocomposite films sintered or annealed in oxygen-containing atmosphere when nanoparticles possessed "metallic core–oxide shell" structure [13–15]. In such a case, considerable effect of

* Corresponding authors. Fax: +48 81 5384575.
E-mail addresses: t.koltunowicz@pollub.pl (T.N. Koltunowicz), p.zhukowski@pollub.pl (P. Zhukowski).

[1] Note that metal-dielectric composites with micrometer and higher sizes of nanoparticles are described by RC equivalent circuits, so that the negative capacitance effect is not observed.

0925-8388/$ - see front matter © 2013 Elsevier B.V. All rights reserved.
http://dx.doi.org/10.1016/j.jallcom.2013.12.125

"negative capacitance" (non-coil-like inductance) can be attributed to the hopping of electrons in weak AC electric field between CoFeZr-based nanoparticles that resulted in the enhancement of matrix polarization [16–19]. As follows from the model reported in [18,19], metallic nanoparticles could be considered as potential wells, and hopping of electrons between neutral wells results in their charging and formation of electric dipoles. Once an electron has jumped from one metallic nanoparticle to another, it stays there for the time τ (much higher that period of AC voltage applied) and only after this time delay it can jump either to the next (third) nanoparticle (as in DC regime) or return to the initial one (in alternating electric field). Probability of the jump to the third particle is p while its hopping back to the first one is $(1-p)$. In the second case, the phase shift is equal

$$\Theta = -\omega\tau. \tag{2}$$

In the low-frequency region it yields negative Θ values, which is the characteristic of the capacitive (RC) circuits. However, for the frequencies

$$f \geqslant \frac{1}{2\tau} \tag{3}$$

the phase shift becomes $\Theta \leqslant -\pi$, due to polarization of matrix and the delay of electron on the second nanoparticle, indicating inductive character of equivalent circuit (RCL) of the studied nanocomposite films.

Previous study performed on granular films with amorphous matrixes (Al_2O_3 or PZT) intrinsically containing oxygen cannot elucidate its role in the formation of "oxide shells" around "metallic cores" of nanoparticles and, consequently, the effect of "negative capacitance" in studied samples. Thereupon, the goal of the paper is to study (f, T) dependences in $(CoFeZr)_x(CaF_2)_{(100-x)}$ nanocomposite films with "core–shell" structure of nanoparticles when dielectric matrix was crystalline and did not contain oxygen.

2. Experimental procedures

Nanocomposite $(CoFeZr)_x(CaF_2)_{(100-x)}$ films with the content of metallic phase 52.2 at.% $\leqslant x \leqslant$ 84.3 at.% were produced by ion-beam sputtering of compound target in a combined argon–oxygen atmosphere in vacuum chamber at partial pressure values of $P_{Ar} = 8.02 \times 10^{-2}$ Pa and $P_O = 9.80 \times 10^{-3}$ Pa, respectively. SEM LEO1455-VP with energy-dispersive Si:Li detector Rontec was used to perform X-ray microanalysis for verification of films composition with accuracy of ~1%. Granular structure of nanocomposites as well as "core–shell" structure of metallic nanoparticles was confirmed using transmission electron microscopy (TEM) at normal and high resolution (HRTEM) [7]. TEM and HRTEM was carried out by Philips EM400T and Philips CM200T microscopes operated at 120 kVand 200 kV, respectively. The Selected Area Electron Diffraction (SAED) patterns were calibrated using crystalline bulk Al and Si references. The data were analyzed with Gatan Digital Micrograph and ELD software.

AC bridge HIOKI 3532 and LCR-meter HiTESTER provided with special PC-based control system was applied for the (f, T), $\Theta(f, T)$ and $C_p(f, T)$ measurements in the frequency range of 42 – 5 MHz.

The as-deposited samples were exposed to testing their electrical properties and then subjected to the 15-min annealing in a tubular furnace in the range of 398 573 K, with the temperature increments of 25 K. After every step of annealing procedure the (f, T), $\Theta(f, T)$ and $C_p(f, T)$ measurements were repeated in the temperature range of 80 K – 373 K, in steps of 5 K.

3. Results and discussion

As was observed in [7] from SEM, TEM, HRTEM, X-ray diffraction analysis and SAED, granular CoFeZr-CaF_2 films sintered in Ar + O_2 atmosphere were characterized by partial or full oxidation of nanoparticles, depending on composition x and partial pressure of oxygen P_O. For example, in the films sintered at $P_O = 4.3 \times 10^{-3}$ Pa α-FeCo(Zr) nanoparticles were covered with oxide shells containing Fe_3O_4 and/or α-Fe_2O_3 phases which were embedded into *crystalline* CaF_2. At the same time, in the samples deposited at $P_O = 9.8 \times 10^{-3}$ Pa the structure of nanoparticles was substantially different. Plan-view HRTEM image of $(CoFeZr)_{38}(CaF_2)_{62}$ film sintered in atmosphere with $P_O = 9.8 \times 10^{-3}$ Pa and correspondent SAED pattern are shown in Fig. 1a and b, respectively.

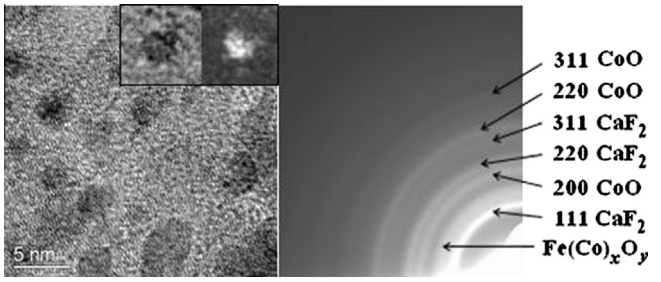

Fig. 1. HRTEM (a) and SAED (b) images of $(CoFeZr)_x(CaF_2)_{(100-x)}$ nanocomposite films, sintered at $P_o = 9.8 \times 10^{-3}$ Pa demonstrating separated nanoparticles inside crystalline CaF_2 matrix. The inset shows bright- and dark-field images of nanoparticle.

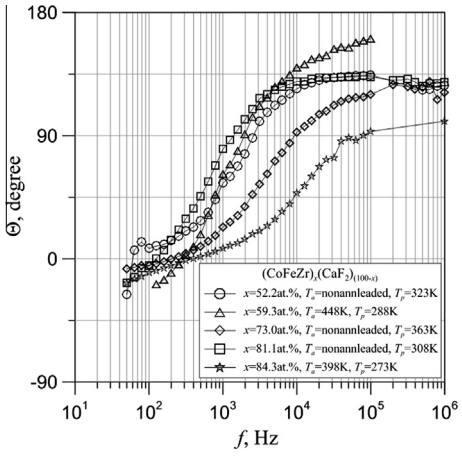

Fig. 2. Phase-shift angle Θ vs. frequency for $(CoFeZr)_x(CaF_2)_{(100-x)}$ nanocomposite films with various metallic-phase content x and for different annealing (T_a) and measuring (T_p) temperatures.

HRTEM image reveals granular structure of film as well as crystalline nature of the nanoparticles seen as dark contrast and CaF_2 matrix seen as grey contrast. SAED pattern of the film shows several narrow rings identified as contribution of CaF_2 matrix and *fcc* crystalline structure of CoO (or FeO) oxide [20] and one broad ring from disordered FeCo-based oxide. Analysis of bright- (BF) and dark-field (DF) TEM images (see the inset in Fig. 1a) clarifies that nanoparticles have "crystalline core–non-crystalline shell" structure. It becomes evident if one compares BF image of nanoparticle as a whole appearing as dark contrast on the background of bright-grey contrast attributed to CaF_2 matrix with DF image that clearly reveals the bright features correspondent to well crystallized core of nanoparticle with diameter smaller than BF image of the same nanoparticle. Formation of nanoparticles with "core–shell" structure is typical for granular films sintered in oxygen-containing atmosphere and was previously confirmed with numerous investigations using complimentary techniques such as TEM, HRTEM and Mössbauer spectroscopy [7].

Behavior of (f, T_p), $\Theta(f, T_p)$ and $C_p(f, T_p)$ dependences could be analyzed taking into account the mentioned above structural differences of the studied films from the observed in $(CoFeZr)_x(Al_2O_3)_{(100-x)}$ and $(CoFeZr)_x(PZT)_{(100-x)}$ samples.

Fig. 2 presents $\Theta(f)$ dependences at temperatures between 270 and 360 K for some as-deposited and annealed samples with varying x. In the low-frequency range the negative Θ values were observed for all the tested samples in the whole measuring

temperature T_p range. When the frequency increases, $\Theta(f)$ curves cross the zero line $\Theta = 0$ and becomes positive. However, the FeCoZr–CaF_2 nanocomposite films were characterized by the Θ values higher than 90° that is impossible to occur in the conventional RLC circuits correspondent to $(CoFeZr)_x(Al_2O_3)$ and $(CoFeZr)_x(PZT)_{(100-x)}$ materials [13,14]. Note that this first peculiarity of $\Theta(f)$ curves was more obviously demonstrated for the samples with x around the percolation threshold. As is seen from Fig. 3a, for the as-deposited sample with $x = 59.3$ at.% measured at $T_p = 323$ K values of Θ were in the range $20° \leqslant \Theta \leqslant 135°$.

Fig. 3b shows the second peculiarity: the dependence of capacitance modulo C_p on frequency exhibits a sharp minimum at the frequency when $\Theta(f)$ curve in Fig. 3a crosses zero line $\Theta = 0$. This agrees with the $C_p(f)$ behavior observed earlier for the $(CoFeZr)_x(Al_2O_3)$ and $(CoFeZr)_x(PZT)_{(100-x)}$ films described in [13,14].

Note also that for the presented $(CoFeZr)_x(CaF_2)_{(100-x)}$ material, as opposed to previous studies [13,14] for $(CoFeZr)_x(Al_2O_3)_{(100-x)}$ and $(CoFeZr)_x(PZT)_{(100-x)}$ films, the maximal Θ values in Fig. 3a exceeded 90° reaching 135° at all temperatures and the highest frequencies.

The third peculiarity consists in the fact that, when the $\Theta(f)$ passed with f increase through the value of 90°, distinct minima were observed on the dependences of real part of admittance on frequency (Fig. 3c). In doing so, the positions of these maxima on (f) curves were shifted to higher f-values when T_p was increased. This is similar to the case of current resonance occurring in the parallel LRC circuits, when the resonance resistance becomes much higher its low-frequency resistance values. Such behavior of (f, T_p) curves means that as the temperature increases, the parallel RCL equivalent circuit (suitable for the description of the composites studied at low temperatures) is transformed at high temperatures into the series equivalent circuit due to the enhance of the permittivity in the material (increase of capacitance contribution in RCL circuit).

Fig. 3c shows that the $lg\sigma(lgf)$ curves display very strong (and close to linear) frequency dependences occurring beyond the position of local resonance minima. Such behavior confirms the

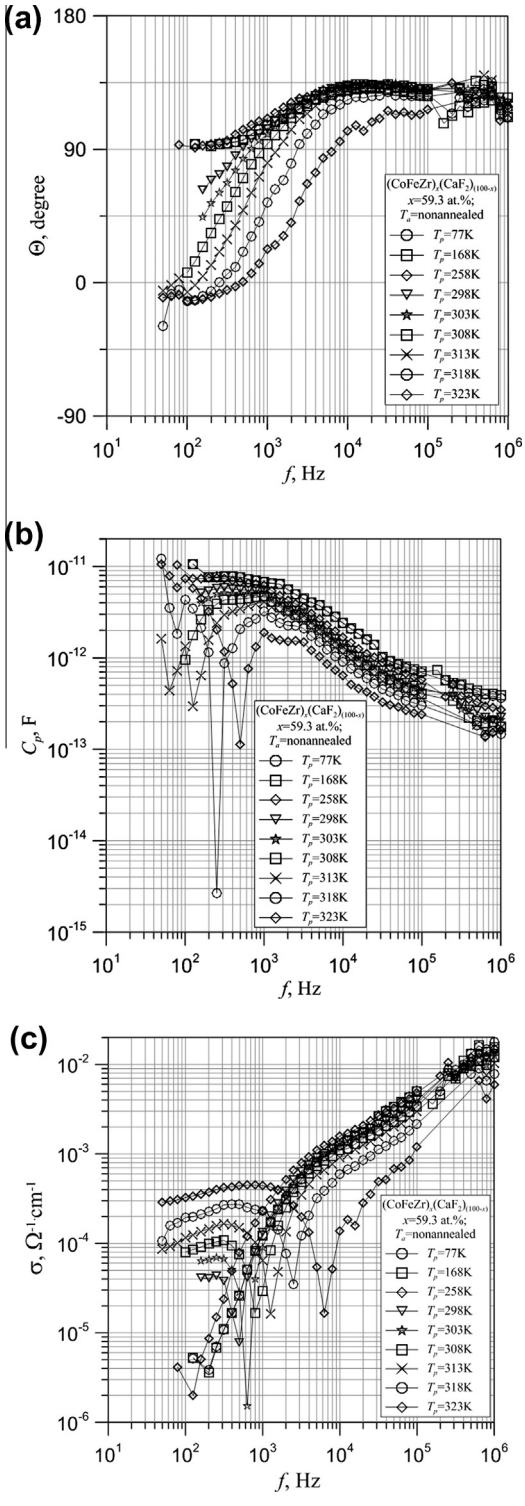

Fig. 3. Frequency dependences of phase-shift angle Θ (a), capacitance C_p (b) and real part of admittance σ (c) for $(CoFeZr)_x(CaF_2)_{(100-x)}$ nanocomposite films with the metallic-phase content of $x = 59.3$ at.%.

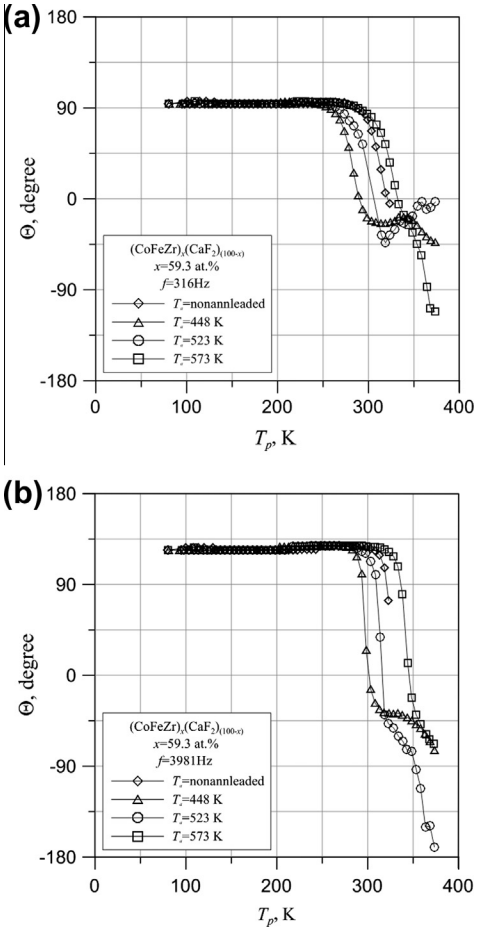

Fig. 4. Phase-shift angle Θ vs. measuring temperature T_p for $(CoFeZr)_x(CaF_2)_{(100-x)}$ nanocomposite films at the frequencies of 316 Hz (a) and 3981 Hz (b).

variable range hopping (tunneling) mechanism of the AC conduction [21] at $f > 10$ kHz. As was mentioned above (see, also [18,19]), hopping of electrons between neutral nanoparticles, resulting in their charging and formation of electric dipoles, draw to the additional thermally-activated polarization of the surrounding dielectric matrix. As far as the electron jump probability p in this model is increased with temperature, the matrix polarization is also increased.

The tendency to the matrix polarization enhancement at $T_p > 250$–280 K also follows from $\Theta(T_p)$ curves in Fig. 4, where capacitive-type admittance becomes dominated at higher values of temperatures and frequencies. Really, comparison of Fig. 4a and b indicates that the low-f inductive-type admittance when $\Theta \approx 90°$ occurs up to $T_p \leqslant 250$ K. However, at higher measuring temperatures the Θ values decrease and at $T_p \approx 280$ K the phase shift angle drops below zero (becomes negative) indicating a transition to the capacitive type of admittance. For the samples with $\Theta > 90°$ (Fig. 4b), these values for high frequencies were observed up to $T_p \approx 290$ K whereupon Θ decreases showing also the transition to the prevailing of capacitive type impedance at higher temperatures.

Note also, that for the samples subjected to stepped heat treatments at $T_a < 448$ K, the $\Theta(T_p)$ dependences shifted to the low temperature region (Fig. 4a and b). It is believed to be due to the fact that, when depositing, part of metallic atoms were dissolved in the dielectric matrix aside of nanoparticles. It was discussed in [6], that during annealing process dissolved atoms diffuse towards nanogranules, formed during deposition, and agglomerate with nanoparticles, that resulted in the reduction of the time τ (owing to granule size increase) and thereby lowering Θ, see relation (2). Annealing at temperatures exceeding 448 K causes surface oxidation of the metallic nanoparticles (and τ increase), shifting the $\Theta(T_p)$ curves to higher temperatures.

Fig. 5 shows the $\sigma(T_p)$ dependences, measured at $f = 316$ Hz and 3981 Hz, after annealing at some selected temperatures. As can be seen, the $\sigma(T_p)$ curves exhibited distinct minima at $\Theta = 90°$, as shown in Fig. 4a and b. Moreover, for the annealing temperatures of 523 K ($f = 3981$ Hz) and 573 K ($f = 316$ Hz), the $\sigma(T_p)$ dependences contained two minima. The first one corresponds to $\Theta_1 = 90°$ and the other one – to $\Theta_2 = -90°$ in $\Theta(T_p)$ curves in Fig. 4. The resistance value in the points of minimal σ values decreased by 10–30 times, depending on the annealing temperature, as compared with σ values at low temperatures. It means that the equivalent circuit for the studied films corresponds to the resonant circuit amplification considerably exceeding 20 dB.

Thus, we have shown that the use of *crystalline oxygen-free fluorite* as dielectric matrix in $(CoFeZr)_x(CaF_2)_{(100-x)}$ nanocomposite films synthesized in mixed argon–oxygen gas atmosphere has brought about essential changes in their electric characteristics as compared with those in $(CoFeZr)_x(Al_2O_3)$ and $(CoFeZr)_x(PZT)_{(100-x)}$ films. In particular, it was observed that the upper limit of phase-shift angle Θ at high frequencies significantly exceeded value of 90° (it varied within the range from −10° to 135°), that never observed in nanocomposites where FeCo-based nanoparticles were embedded into Al_2O_3 or PZT dielectric matrixes. This display the enhancement of thermally-activated polarization of the surrounding dielectric matrix around nanoparticles due to their recharging during hopping of electrons. In our opinion, there are two possible reasons for this effect in the studied films: (1) the participation of fluorine in the formation of "oxide shells" around the metallic nanoparticles, and/or (2) the crystalline form of CaF_2 matrix.

As to the first reason, during the sputtering of the fluoride-containing compound target, a part of the fluorine ions can be released from CaF_2. Getting to the gas atmosphere in vacuum chamber, these ions together with the oxygen ones can participate in the formation of FeCo-based oxide "shells" during sputtering process producing additional chemical reactions with the metallic atoms. These changes in the composition of "shells" around the metallic nanoparticles can probably cause the increase in time delay τ at hopping process and thereby extending the range of the Θ values variation up to its upper level reaching $\Theta = 135°$ at the highest frequencies.

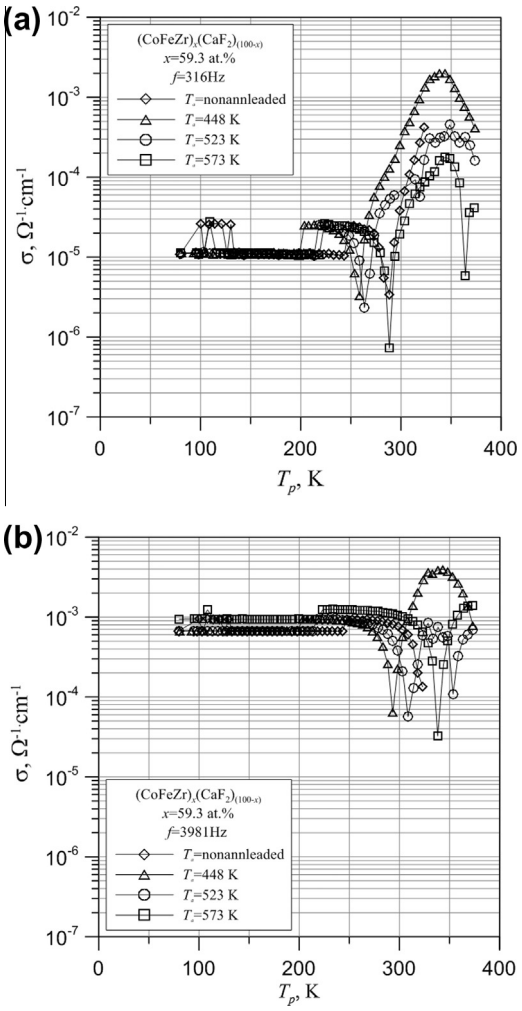

Fig. 5. Real part of admittance σ vs. measuring temperature T_p for $(CoFeZr)_x(CaF_2)_{(100-x)}$ nanocomposite films at the frequencies of 316 Hz (a) and 3981 Hz (b).

On the other side, crystalline form of fluorite (argued by electron and X-ray diffraction [7]), in nanocomposites studied can also enhance its polarization by the charged nanoparticles during the hopping process, as opposed to the amorphous alumina or PZT matrixes. The last can also result in strong increase of τ and, as a consequence, Θ values, see Eq. (2). However, we should note that the above described measurements did not fixed features of F-containing compounds in the samples studied. Now, additional experiments and more detailed analysis of fluorine and fluorite role are needed to understand which of the above reasons can dominate in the AC conductance behavior of $(CoFeZr)_x(CaF_2)_{(100-x)}$ nanocomposite films our case.

4. Resume

The obtained results have shown strong difference in behavior of AC conductance of $(CoFeZr)_x(CaF_2)_{(100-x)}$ nanocomposite films, synthesized in mixed argon–oxygen gas atmosphere, as compared with those in $(CoFeZr)_x(Al_2O_3)$ and $(CoFeZr)_x(PZT)_{(100-x)}$ films. This

difference consists of two peculiarities observed on the (f, T), $\Theta(f, T)$ and $C_p(f, T)$ dependences of $(CoFeZr)_x(CaF_2)_{(100-x)}$ samples: (1) the $\Theta(f, T)$ values at high frequencies could be approached the values of 135°, while in nanocomposites where FeCo-based nanoparticles were embedded into alumina or PZT matrixes; (2) the $\sigma(T_p)$ curves for the annealed samples exhibited two minima corresponding to $\Theta_1 = 90°$ and $\Theta_2 = -90°$ values in $\Theta(f)$ curves. Such behavior of the films studied in this paper can be attributed either participation of fluorine in the formation of "oxide shells" around the metallic nanoparticles, or/and the crystalline form of CaF_2 matrix: both of them can result in the enhancement of matrix polarization and increase the life time of electrons on nanoparticles. But, in any case, we have shown that we can tune the AC conductance behavior in metal-dielectric nanocomposite films (domination either capacitive- or inductive-like contributions) changing their composition (type of dielectric matrix, content of metallic phase nanoparticles and type of shells around them), and also measuring and annealing temperatures.

Acknowledgements

The work and investigations were carried out as a research project No IP2012 026572 within the Iuventus Plus program of Polish Ministry of Science and Higher Education in the years of 2013-2015. Authors from Belarus would like additionally to thank Visby Program of Swedish Institute and the State Sub-Programme "Crystalline and molecular systems" of Belarus for financial support during years of 2011-2013.

References

[1] A.D. Pogrebnjak, M.M. Danilionok, V.V. Uglov, N.K. Erdybaeva, G.V. Kirik, S.N. Dub, V.S. Rusakov, A.P. Shypylenko, P. Zukovski, Y.Z. Tuleushev, Vacuum 83 (2009) S235–S239.

[2] A.D. Pogrebnjak, A.P. Shpak, G.V. Kirik, N.K. Erdybaeva, M.V. Il'yashenko, A.A. Dem'yanenko, Y.A. Kunitskii, A.S. Kaverina, V.S. Baidak, N.A. Makhmudov, P.V. Zukowski, F.F. Komarov, V.M. Beresnev, S.M. Ruzimov, A.P. Shypylenko, Acta Phys. Pol. A 120 (1) (2011) 94–99.

[3] R.S. Iskhakov, S.V. Komogortsev, E.A. Denisova, Yu.E. Kalinin, A.V. Sitnikov, JETP Lett. 86 (7) (2007) 465–469.

[4] R.S. Iskhakova, E.A. Denisova, S.V. Komogortsev, L.A. Chekanova, Yu.E. Kalinin, A.V. Sitnikov, Phys. Solid State 52 (11) (2010) 2263–2266.

[5] P. Zhukowski, J. Sidorenko, T.N. Kołtunowicz, J.A. Fedotova, A.V. Larkin, Przegl. Elektrotechniczny 86 (7) (2010) 296–298.

[6] P. Zhukowski, T.N. Kołtunowicz, J.A. Fedotova, A.V. Larkin, Przegl. Elektrotechniczny 86 (7) (2010) 157–159.

[7] T.N. Koltunowicz, P. Zukowski, M. Milosavljević, A.M. Saad, J.V. Kasiuk, J.A. Fedotova, Yu.E. Kalinin, A.V. Sitnikov, A.K. Fedotov, J. Alloys Comp. 586 Supplement 1 (2014) S353–S356, http://dx.doi.org/10.1016/j.jallcom.2012.09.121.

[8] P. Zukowski, T. Kołtunowicz, J. Partyka, Yu A. Fedotova, A.V. Larkin, Vacuum 83 (1) (2009) S280–S283.

[9] H.L. Kwok, Solid-State Electron. 47 (6) (2003) 1089–1093.

[10] H.L. Kwok, Phys. Status Solidi 5 (2) (2008) 638–640.

[11] L. Bakueva, G. Konstantatos, S. Musikhin, H.E. Ruda, A. Shika, Appl. Phys. Lett. 85 (16) (2004) 3567–3569.

[12] M. Ershov, H.C. Liu, L. Li, M. Buchanan, Z.R. Wasilewski, A. Jonscher, IEEE Trans. Electron Dev. 45 (10) (1998) 2196–2206.

[13] P. Zhukowski, T.N. Kołtunowicz, P. Wegierek, J.A. Fedotova, A.K. Fedotov, A.V. Larkin, Acta Phys. Pol. A 120 (1) (2011) 43–45.

[14] T.N. Kołtunowicz, J.A. Fedotova, P. Zhukowski, A. Saad, A. Fedotov, J.V. Kasiuk, A.V. Larkin, J. Phys. D: Appl. Phys. 46 (12) (2013) 125304.

[15] T.N. Kołtunowicz, P. Zhukowski, A.K. Fedotov, A.V. Larkin, A. Patryn, B. Andriyevskyy, A. Saad, J.A. Fedotova, V.V. Fedotova, Elektronika ir Elektrotechnika (Electron. Electr. Eng.) 19 (4) (2013) 37–40.

[16] P. Zukowski, T. Koltunowicz, J. Partyka, P. Wegierek, F.F. Komarov, A.M. Mironov, N. Butkievith, D. Freik, Vacuum 81 (10) (2007) 1137–1140.

[17] T.N. Kołtunowicz, P. Zhukowski, V.V. Fedotova, A.M. Saad, A.K. Fedotov, Acta Phys. Pol. A 120 (1) (2011) 39–42.

[18] P.W. Zukowski, A. Rodzik, Y.A. Shostak, Semiconductors 31 (6) (1997) 610–614.

[19] P.V. Zukowski, J. Partyka, P. Wagierek, Yu. Shostak, Yu. Sidorenko, A. Rodzik, Semiconductors 34 (10) (2000) 1124–1127.

[20] R.M. Cornell, U. Schwertmann, The Iron Oxides: Structure, Properties, Reactions, Occurrences and Uses, Wiley-VCH Verlag, Weinheim, 2003. 703 p.

[21] N.F. Mott, E.A. Davis, Electron Process in Non-Crystalline Materials, Claredon Press, Oxford, 1979.